Dynamical Density Functional Study of the Multistep CO Insertion into Zirconium−Carbon Bonds Anchored to a Calix[4]arene Moiety

S. Fantacci, F. De Angelis,† and A. Sgamellotti*

Dipartimento di Chimica e Centro di Studio CNR per il Calcolo Intensivo in Scienze Molecolari, Università di Perugia, I-06123 Perugia, Italy

N. Re

Facoltà di Farmacia, Università G. D'Annunzio, I-66100 Chieti, Italy

Received June 13, 2001

The multistep migratory insertion reaction of CO into the zirconium−carbon bonds in [calix[4](OMe)$_2$(O)$_2$ZrMe$_2$] has been investigated by means of both static and dynamic density functional calculations. A relatively stable facial CO complex has been observed with a negligible barrier for CO insertion into one of the Zr−Me bonds, leading to the formation of an η^2-acyl complex. The insertion of the residual alkyl group into the acyl moiety, leading to an η^2-bound acetone, has also been investigated, and a small energy barrier, 2.3 kcal/mol, has been found. Dynamics simulations have been performed on the [calix[4](OMe)$_2$(O)$_2$Zr(Me)$_2$]−CO adduct in order to study the detailed features of the whole multistep insertion and show that the migratory insertion leads to the formation of an out-of-plane η^1-acyl complex, which is readily converted into the more stable η^2-acyl isomer within 1.5 ps. The subsequent methyl to acyl migration has been observed within 5 ps, leading to the formation of the η^2-bound acetone by a facial attack of the migrating methyl to the acyl carbon. A comparison with the migratory insertion of CO into the metal−alkyl bond in (Me)$_2$Zr(Cp)$_2$ has been performed, showing substantial differences in the reactivity of the calix[4]arene and bis(cyclopentadienyl) substrates.

Introduction

The migratory insertion of carbon monoxide into metal−alkyl and metal−hydride bonds is an important organometallic reaction that has been extensively studied by synthetic, mechanistic, and theoretical points of view.[1−7]

The insertion of carbon monoxide in metal−alkyl bonds has been observed for most of the early d-block metals as well as numerous actinide and lanthanide elements. Spectroscopic data and structural studies have indicated that all isolable CO insertion products contain η^2-acyl groups, where both carbon and oxygen atoms are bound to the metal center (see Scheme 1). The unique reactivity of the coordinated acyls has been attributed to this η^2-bonding mode. In particular, several studies on the reaction of CO with (Cp)$_2$Zr(Me)$_2$ have shown that the η^2-acyl moiety lies in the symmetry plane bisecting the Cp−M−Cp angle and may assume two different orientations, one with the oxygen atom directed away from the additional ligand X and the other with the oxygen directed toward X (conventionally indicated as, respectively, "O-outside" and "O-inside").[10,11]

Scheme 1

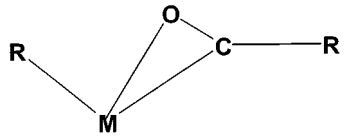

Isolated η^2-acyl complexes are very reactive and undergo a variety of interesting transformations,[11] such as the insertion of the alkyl group into the acyl moiety, to generate a η^2-ketone,[12] or the uptake of a second CO molecule to give an enediolate.[13]

Recently, it has been reported the multistep migratory insertion of carbon monoxide into the metal−carbon bonds of the ZrR$_2$ fragment anchored to a tetraoxo matrix, defined by the dimethoxycalix[4]arene dianion

† Present address: Department of Chemistry, Princeton University, Princeton, NJ 08544, and Princeton Materials Institute, Princeton University, Princeton, NJ 08544.

(1) Calderazzo, F.; *Angew. Chem., Int. Ed. Engl.* **1977**, *16*, 299.
(2) Kulhmann, E. J.; Alexander, J. J. *Coord. Chem. Rev.* **1980**, *33*, 195.
(3) Wojcicki, A. *Adv. Organomet. Chem.* **1973**, *11*, 97.
(4) Foold, T. C. In *Topics in Stereochemistry*; Geoffry, G. L., Ed.; Wiley: New York, 1981; Vol. 12, p 83.
(5) Alexander, J. J. In *The Chemistry of the Metal−Carbon Bond*; Hartley, F. R., Ed.; Wiley: New York, 1985; Vol. 2.
(6) Bock, P. L.; Boschetto, D. J.; Rasmussen, J. R.; Demeres, J. P.; Whitesides, G. M. *J. Am. Chem. Soc.* **1974**, *96*, 2814.
(7) Wax, M. J.; Bergman, R. G.; *J. Am. Chem. Soc.* **1981**, *103*, 7028.
(8) Facchinetti, G.; Floriani, C. *J. Organomet. Chem.* **1974**, *71*, C5.
(9) Facchinetti, G.; Fochi, G.; Floriani, C. *J. Chem. Soc., Dalton Trans.* **1977**, 1946.
(10) Erker, G. *Acc. Chem. Res.* **1984**, *17*, 103.
(11) Durfee, L. D.; Rothwell, I. P. *Chem. Rev.* **1988**, *88*, 1059.
(12) Erker, G.; Rosenfeldt, F. *J. Organomet. Chem.* **1982**, *224*, 29−42.
(13) Manriquez, J. M.; McAlister, D. R.; Sanner, R. D.; Bercaw, J. E. *J. Am. Chem. Soc.* **1978**, *100*, 2716. Hofmann, P.; Stauffert, P.; Frede, M.; Tatsumi, K. *Chem. Ber.* **1989**, *122*, 1559.

10.1021/om010509i CCC: $20.00
Publication on Web 09/10/2001

Scheme 2

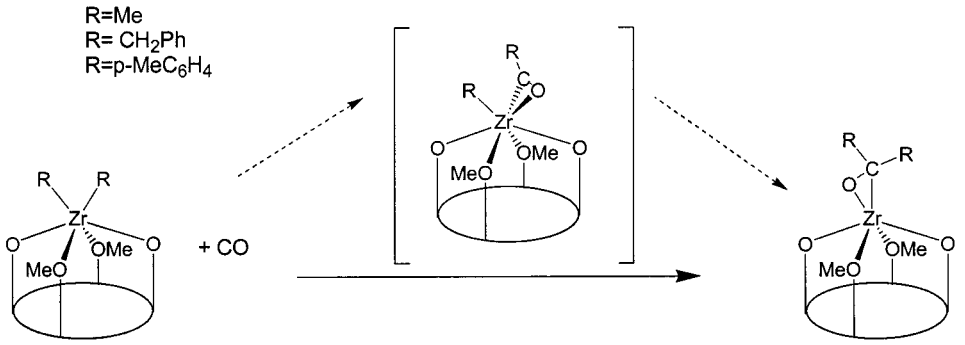

[*p*-Bu^t-calix[4]-(OMe)$_2$(O)$_2$]$^{2-}$.[14] Relevant differences have been observed between the CO reaction with [*p*-Bu^t-calix[4]-(OMe)$_2$(O)$_2$ZrR$_2$] and that with the analogous (Cp)$_2$ZrR$_2$ complex. Unlike those for the bis(cyclopentadienyl) zirconium derivatives, the reaction of CO with [*p*-Bu^t-calix[4]-(OMe)$_2$(O)$_2$ZrR$_2$] [R = Me,CH$_2$Ph, *p*-MeC$_6$H$_4$] has been proposed to proceed via a two-step migration to give directly the corresponding η^2-ketones [*p*-Bu^t-calix[4]-(OMe)$_2$(O)$_2$Zr(R$_2$CO)]. The formation of these ketones has been postulated to occur via the intermediacy of an η^2-acyl species (see Scheme 2), which, at variance with the bis(cyclopentadienyl) zirconium derivatives, could not be detected.

To cast some light onto the reaction mechanism of the multistep CO insertion into the zirconium−alkyl bond in [*p*-Bu^t-calix[4]-(OMe)$_2$(O)$_2$ZrMe$_2$], we combined "static" gradient-corrected DFT calculations on the stationary points of the potential surface with first-principles molecular dynamics calculations based on the Car−Parrinello approach.[15] We optimized the geometries of all the minima involved in the insertion reaction and localized the transition states for the key steps of the overall considered reaction leading to the η^2-bound [*p*-Bu^t-calix[4]-(OMe)$_2$(O)$_2$Zr(Me$_2$CO)] acetone complex. Car−Parrinello simulations have been employed to study the detailed dynamical features of (i) the carbonyl migratory insertion from the [*p*-Bu^t-calix[4]-(OMe)$_2$-(O)$_2$ZrMe$_2$]−CO adduct to the η^2-acyl complex and (ii) the subsequent methyl-to-acyl migration from the zirconium−acyl complex.

Computational Details

Static DFT Calculations. The static DFT calculations reported in this paper are based on the ADF (Amsterdam Density Functional) program package described elsewhere.[16,17] Its main characteristics are the use of a density fitting procedure to obtain accurate Coulomb and exchange potentials in each SCF cycle, the accurate and efficient numerical integration of the effective one-electron Hamiltonian matrix elements, and the possibility to freeze core orbitals. The frozen cores have been 1s4p for Zr and 1s for C and O. The molecular orbitals were expanded in an uncontracted DZ STO basis set for all atoms with the exception of the transition metal orbitals, for which we used a DZ STO basis set for 4s and 4p and a TZ STO basis set for 4d and 5s. As polarization functions, one 5p, one 3d, and one 2p STO were used for Zr, O, and H, respectively. A set of 3d polarization functions was also placed on the carbon atoms belonging to the methyl and carbonyl groups bound to the metal. Geometry optimizations were performed on all the stationary points of the potential energy surface for the CO insertion, considering the Vosko−Wilk−Nusair LDA parametrization[18] and including the Becke[19] and Perdew−Wang[20] gradient corrections (GC) to the exchange and correlation, respectively.

The energy profiles for the CO coordination process, as well as those for the CO insertion and for the η^2-acyl → η^2-ketone conversion, have been traced by means of linear transit calculations, and the transition states for the key steps of the overall reaction have been located starting from the maximum energy structures encountered during the linear transit procedure, using the Powell method[21] implemented in the ADF package. For the bimolecular coordination process we evaluated the basis set superposition error (BSSE).

Car−Parrinello Calculations. Molecular dynamics simulations were carried out with the Car−Parrinello (CP) method.[22,23] For the LDA exchange−correlation functional the Perdew−Zunger parametrization[24] has been used, while the gradient-corrected functional is taken from ref 25. Core states are projected out using pseudopotentials. For Zr, C, O, and H "ultra-soft" pseudopotentials were generated according to the scheme proposed by Vanderbilt.[23] The wave functions were expanded in plane waves up to an energy cutoff of 25 Ry. Periodic boundary conditions were used by placing the model molecule in a cubic box of 15.87 Å, keeping a minimum of 5.0 Å between repeated images, sufficiently large to avoid any coupling between periodic images. The equations of motion were integrated using a time step of 6 au (0.145 fs) with an electronic fictitious mass $\mu = 2000$ au.

To check the consistency of the CP and ADF programs, we compared the geometries of the model [calix[4](OMe)$_2$(O)$_2$Zr-(Me)$_2$] complex **1**, optimized at both levels of theory, with that of [*p*-Bu^t-calix[4](OMe)$_2$(O)$_2$−Zr(CH$_2$Ph)$_2$], the closest experimental compound, for which X-ray data are available.[14] Table 1 shows a good agreement between the two approaches and experimental data, suggesting that metal−ligand interactions are accounted for with the same accuracy within both approaches.

(14) Giannini, L.; Caselli, A.; Solari, E.; Floriani, C.; Chiesi-Villa, A.; Rizzoli, C.; Re, N.; Sgamellotti, A. *J. Am. Chem. Soc.* **1997**, *119*, 9709.
(15) Car, R.; Parrinello, M. *Phys. Rev. Lett.* **1985**, *55*, 2471.
(16) Ziegler, T.; Tshinke, V.; Baerends, E. J.; Snijders, J. G.; Ravenek, W. *J. Phys. Chem.* **1989**, *93*, 3050.
(17) (a) Baerends, E. J.; Ellis, D. E.; Ros, P. *Chem Phys.* **1973**, *2*, 42. (b) Baerends, E. J.; Ros, P. *Chem Phys.* **1973**, *2*, 51. (c) Baerends, E. J.; Ros, P. *Chem Phys.* **1975**, *8*, 41. (d) Baerends, E. J.; Ros, P. *Int. J. Quantum Chem.* **1978**, *S12*, 169.
(18) Vosko, S. H.; Wilk, L.; Nusair, M. *Can. J. Phys.* **1980**, *58*, 1200.
(19) Becke, A. D. *Phys. Rev.* **1988**, *A38*, 3098.
(20) Perdew, J. P.; Wang, Y. *Phys. Rev.* **1992**, *B45*, 13244.
(21) Powell, M. J. D. *Math. Prog.* **1977**, *12*, 241.
(22) The implementation that we use is described in: Pasquarello, A.; Laasonen, K.; Car, R.; Lee, C.; Vanderbilt, D. *Phys. Rev. Lett.* **1992**, *69*, 1982. Pasquarello, A.; Laasonen, K.; Car, R.; Lee, C.; Vanderbilt, D. *Phys. Rev. B* **1993**, *47*, 10142.
(23) Vanderbilt, D. *Phys. Rev. B* **1990**, *41*, 7892.
(24) Perdew, J. P.; Zunger, A. *Phys. Rev. B* **1981**, *23*, 5048.
(25) Perdew, J. P.; Chevary, J. A.; Vosko, S. H.; Jackson, K. A.; Pederson, M. R.; Singh, D. J.; Fiolhais, C. *Phys. Rev. B* **1992**, *46*, 6671.

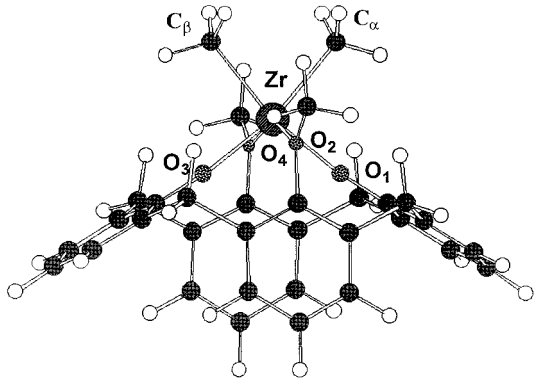

1

Figure 1. Optimized structure of the [calix[4]-$(OMe)_2$-$(O)_2ZrMe_2$] complex **1**.

Table 1. Optimized Geometrical Parameters (Å and deg) of [Calix[4]$O_2(OMe)_2Zr(CH_3)_2$], 1, Using the ADF and CP Programs, Compared with X-ray Data Observed for the Dimethyl Complex[14]

parameter	ADF	CP	expt[14]
$R_{ZrO_{1,3}}$	2.060	2.020	1.960
$R_{ZrO_{2,4}}$	2.389	2.366	2.298
$R_{O_{1,3}C_1}$	1.329	1.344	
$R_{O_{2,4}C_2}$	1.427	1.434	
$R_{ZrC_{\alpha,\beta}}$	2.336	2.323	2.332
$\angle O_1ZrO_3$	104.7	104.3	102.4
$\angle O_2ZrO_4$	154.5	154.7	153.9
$\angle ZrO_1C_1$	174.3	174.1	175.9
$\angle ZrO_2C_2$	113.3	113.4	118.2
$\angle C_\alpha ZrC_\beta$	79.1	79.4	83.7

Results and Discussion

The [*p*-Bu^{t}calix[4]$(OMe)_2(O)_2Zr(Me)_2$] is the starting reactant of the considered CO migrative insertion. We modeled the experimental complex with [calix[4]$(OMe)_2$-$(O)_2Zr(Me)_2$], **1**, where the Bu^t groups in para position are substituted by H atoms. It has been shown that for this class of compounds this approximation does not affect the electronic properties of the investigated systems.[26] We optimized the geometry of complex **1** under C_{2v} symmetry constraints and the computed structure is plotted in Figure 1, in which the two methyl carbon atoms bound to the metal center lie in the *yz* plane. Hereafter we will refer to C_α,C_β as the carbon atoms of the methyl groups (respectively, that undergoing the CO insertion and the remaining one), O_1,O_3 as the phenoxo oxygens, and O_2,O_4 as the methyl phenoxo oxygens; see Figure 1. Optimized parameters, obtained using the ADF and CP programs, are compared with X-ray data for [*p*-Bu^t-calix[4]$(OMe)_2(O)_2Zr(CH_2Ph)_2$] in Table 1. The d^0 dimethyl complex **1** shows a distorted octahedral coordination of the six ligands around the metal center; the $Zr-O_{2,4}$ bond lengths indicate a weak coordination, while the $Zr-O_{1,3}$ bonds show a multiple bond character, as reflected by the quasi linear $\angle Zr-O_{1,3}-C_{1,3}$ angle (see Table 1). The computed geometries are in very good agreement with the experimental structure. Only the $Zr-O_{2,4}$ distances show significant deviations (0.09−0.07 Å, ADF and CP, respectively) but may be connected with the weak interaction between these ether oxygens and the metal center, which makes these distances susceptible to the replacement of the ^{t}Bu groups with hydrogen atoms.

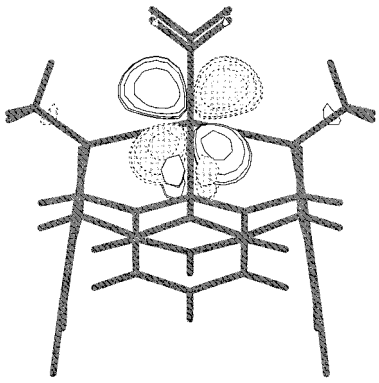

Figure 2. Isodensity surface plot of the LUMO orbital of [calix[4]-$(OMe)_2(O)_2ZrMe_2$] complex.

CO Coordination by the Metal. The initial step of the migratory insertion reaction is supposed to be the coordination of the electrophilic CO molecule to the electron-deficient metal center. Frontier orbital analysis of the [calix[4]-$(OMe)_2(O)_2ZrMe_2$] complex **1** shows an isolated LUMO ($24b_1$) with an essentially zirconium d_{xz} character; see Figure 2. In agreement with previous extended Hückel calculations,[14] this is the only vacant molecular orbital to which the incoming CO ligand can donate prior to insertion, and its spatial extension suggests that the most favorable approach of CO occurs along a line in the plane bisecting the Me−Zr−Me angle (*xz*) forming an angle of ca. 45° with the *z* axis, A in Scheme 3, and leads to a facial CO adduct. Note that this is a quite different situation from that observed for the CO attack to bis(cyclopentadienyl) metal dialkyl complexes, where the carbon monoxide attack may occur within the Me−M−Me plane (*yz*), along the *z* axis ("central" attack, B), or perpendicularly to it ("lateral" attack, C) and leads to meridional CO adducts;[27] see Scheme 3. This difference is due to the peculiar frontier orbital scheme of the bent bis(cyclopentadienyl) metal fragment, which shows three coplanar low-lying metal orbitals ($1a_1$, $1b_1$, $2a_1$) pointing in the symmetry plane bisecting the Cp−M−Cp angle[28] and forces the three additional L ligands of Cp_2ML_3 species to assume a meridional geometry.[28−30] On the other hand, the [calix-[4]-$(OMe)_2(O)_2Zr]^{2+}$ fragment shows four non-coplanar low-lying metal orbitals, $1a_1(d_{z^2})$, $1b_1(d_{xz})$, $1b_2(d_{yz})$, and $1a_2(d_{xy})$, which favor a facial geometry of the three additional L ligands of the [calix[4]-$(OMe)_2(O)_2ZrL_3$] species.[14]

To check this point, geometry optimizations were performed on the [calix[4]-$(OMe)_2(O)_2Zr(CO)Me_2$] complex with the expected facial geometry without any symmetry constraints and also with two possible meridional geometries (one of C_{2v} symmetry with the CO lying between the two methyl groups and one of C_s symmetry with the CO placed on the side of one methyl group; see Figure 3). The facial geometry **2a** was found

(26) Fantacci, S.; Sgamellotti, A.; Re, N.; Floriani, C. *J. Chem. Soc., Dalton Trans.* **2001**, 1718.

(27) De Angelis, F.; Sgamellotti, A.; Re, N. *Organometallics* **2000**, *23*, 4904. De Angelis, F.; Sgamellotti, A.; Re, N. *Organometallics* **2001**, *20*, 1486.

(28) Lauher, J. W.; Hoffmann, R. *J. Am. Chem. Soc.* **1976**, *98*, 1729.

(29) Tatsumi, K.; Nakamura, A.; Hofmann, P.; Stauffert, P.; Hoffmann, R. *J. Am. Chem. Soc.* **1985**, *107*, 4440.

(30) Hofmann, P.; Stauffert, P.; Tatsumi, K.; Nakamura, A.; Hoffmann, R. *Organometallics* **1985**, *4*, 404.

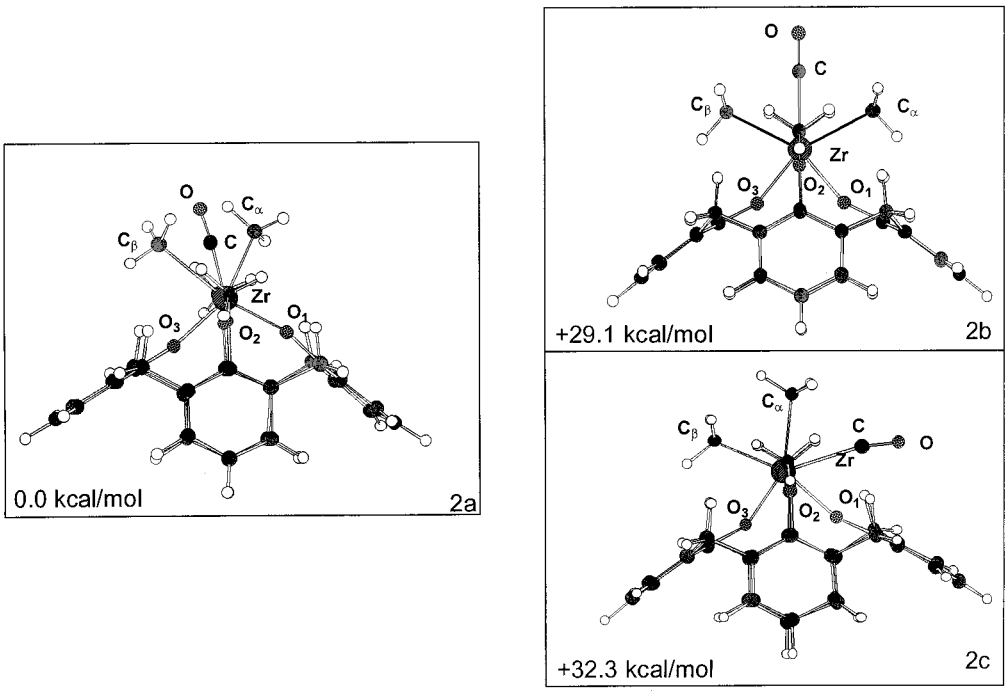

Figure 3. Optimized structures and relative stability of the three CO-adducts **2a**, **2b**, and **2c**.

Scheme 3

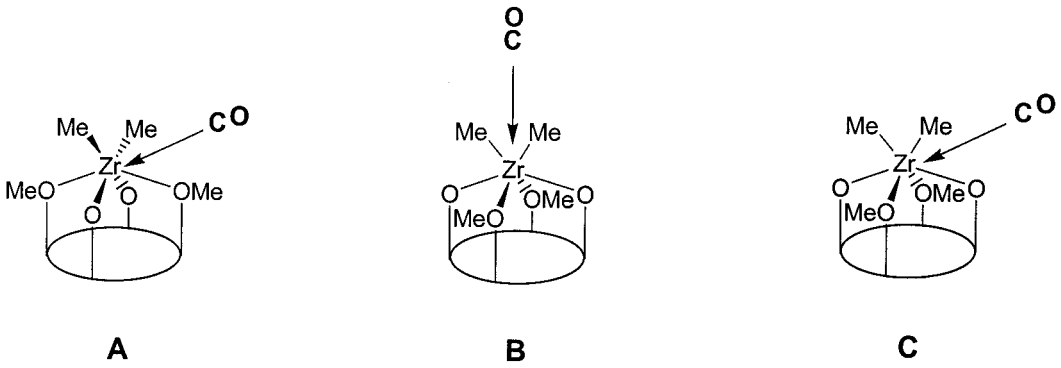

the lowest in energy, 11.1 kcal/mol (7.4 kcal/mol when accounting for BSSE correction) below the free reagents, with the "central" **2b** and "lateral" **2c** meridional isomers 29.1 and 32.3 kcal/mol higher in energy, respectively, therefore not stable with respect to the free reagents. Moreover, both meridional structures relaxed to the facial one as soon as the C_{2v} or C_s symmetry constraints were removed, showing that the latter is the only stable dimethyl carbonyl adduct.

The optimized geometry of the facial CO-adduct **2a** (see Table 2) shows a long Zr−C(CO) distance, 2.216 Å, suggesting quite a weak interaction between the CO ligand and the [calix[4]-$(OMe)_2(O)_2ZrMe_2$] fragment, as expected since the CO ligand cannot exploit any stabilizing π back-donation interaction with a d^0 electron-deficient metal center such as Zr(IV). The Zr−C(Me) distances were 2.473 and 2.459 Å, significantly longer than in the dimethyl complex (2.336 and 2.323 Å). The lengthening of these bond distances reflects the geometrical perturbation due to CO coordination and prepares the methyl groups for the carbonyl insertion. The structures of **2a**, **2b**, and **2c** have been illustrated in Figure 3, while a list of main optimized geometrical parameters for **2a** have been reported in Table 2.

Table 2. Optimized Geometrical Parameters (bond lengths in Å and angles in deg) of CO Adduct 2a, η^1-Acyl Complex 3, η^2-Acyl Complex 4a, and the Transition State for the Formation of Ketone from the η^2-Acyl Complex

parameter	**2a**	**3**	**4a**	$TS_{4a\rightarrow 5}$
R_{Zr-O_1}	2.045	2.022	2.049	2.056
R_{Zr-O_2}	2.415	2.369	2.388	2.349
R_{Zr-O_3}	2.050	2.063	2.070	2.060
R_{Zr-O_4}	2.561	2.455	2.421	2.417
R_{Zr-C_α}	2.473	3.051		
R_{Zr-C_β}	2.459	2.347	2.384	2.398
R_{Zr-CO}	2.216	2.330	2.231	2.212
R_{Zr-O}			2.280	2.294
R_{C-O}	1.167	1.227	1.262	1.291
$R_{C_\alpha-CO}$	2.259	1.555	1.492	1.489
$\angle O_1ZrO_3$	106.7	125.8	110.0	112.0
$\angle O_2ZrO_4$	150.3	157.0	152.0	152.2
$\angle C_\alpha CZr$	67.1	101.6	163.5	160.9
$\angle CZrC_\beta$	62.8	68.8	71.8	64.7
$\angle ZrCO$	176.5	140.2	75.9	77.3
$\angle OCZrC_\beta$	22.6	91.5	97.5	102.5

To check the presence of an energy barrier to CO coordination, we performed a linear transit scan of the potential energy surface of the [calix[4]-$(OMe)_2(O)_2Zr$] + CO system, assuming the CO carbon−zirconium distance as a reaction coordinate. Constrained geometry

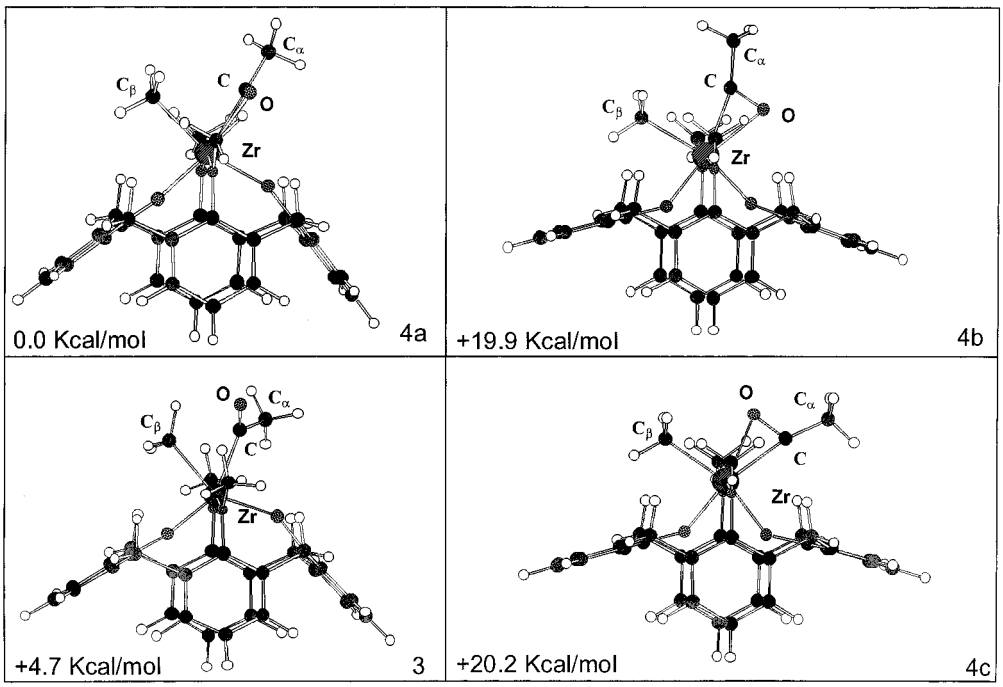

Figure 4. Optimized structures of the acyl complexes **3**, **4a**, **4b**, and **4c**.

optimizations without any symmetry were performed by keeping fixed the Zr−CO distance at selected values in the range 4.0−2.2 Å and relaxing all the other geometrical parameters. The potential energy curve for the CO attack (see Figure S1) shows an almost negligible barrier to coordination of 2.0 kcal/mol. It is worth noting that this barrier is smaller than that calculated for the $(Cp)_2Zr(CH_3)_2$ + CO system, 2.0 vs 7.5 kcal/mol.[27] Moreover for the latter system the most favorable CO attack was found to be the "lateral" one, C in Scheme 3, leading to a meridional CO adduct[27] and not to the facial CO adduct 2a.

CO Insertion and Acyl Complexes. Both η^1- and η^2-bound acyl complexes may assume two possible conformations with the acyl moiety lying in the $Zr-O_2$ plane (*yz*) containing the uninserted methyl ("in-plane") or with the acyl moiety lying out of this plane ("out-of-plane"). Moreover the in-plane conformation may show two different orientations, one with the oxygen atoms directed away from the uninserted methyl and one with the oxygen atom directed toward the uninserted methyl. According to the nomenclature conventionally used for the $Cp_2M(\eta^2\text{-RCO})X$ systems, these two orientations will be indicated as respectively "O-outside" and "O-inside". We optimized the geometry of the η^1-, **3**, and η^2-bound acyl complexes, **4a**, without any symmetry constraints, finding two "out of plane" structures, with the CO group lying almost perpendicular to the *yz* plane. The computed structures are plotted in Figure 4, and the main geometrical parameters are reported in Table 2; the optimized parameters for the calixarene moiety are similar in **3** and **4a**, except for the $\angle O_1ZrO_3$ angle, which is larger for the η^1-acyl complex (125.8° vs 110.0°), reflecting the flexibility of the calixarene tetradentate ligand, which can rearrange on the basis of the different metal coordination. We found the η^1-isomer **3** 14.7 kcal/mol below the CO adduct **2a** and the η^2-bound isomer **4a** still 4.7 kcal/mol lower in energy. We therefore see that the migratory CO insertion into the Zr−methyl bond is a thermodynamically favorable process by 19.4 kcal/mol. For the sake of completeness, we also considered the in-plane η^1- and η^2-acyl complexes, both in O-outside and O-inside orientations, performing geometry optimizations within C_s symmetry constraints. We found the two η^2-acyl isomers, in the O-outside, **4b**, and O-inside, **4c**, configurations, almost isoenergetic and 19.9 and 20.2 kcal/mol, respectively, above the out-of-plane η^2-isomer **4a**. The O-inside η^1-isomer **4d** was calculated 10.0 kcal/mol higher in energy than **4c**, while no stable O-outside η^1-structure was found. Structures and the relative energies of the η^1- and η^2-acyl complexes can be found in Figure 4.

We then searched for the energy barrier of the migratory insertion reaction which properly correlates the facial CO adduct **2a** with the η^1-acyl complex **3** by performing a linear transit scan of the potential energy surface starting from **2a**, assuming the $CO-CH_3$ carbon−carbon distance as a reaction coordinate in the range 1.5−2.2 Å. The calculated curve (see Figure S2) shows a maximum only 0.9 kcal/mol higher than **2a**, 10.2 kcal/mol below the free reagents, for a carbon−carbon distance of ca. 1.8 Å. Such a negligible overestimate of the energy barrier suggests that there is probably no transition state for the migratory insertion from the facial CO adduct **2a**.

Dynamics Calculations. We started the dynamics simulation of the migratory insertion reaction by heating the structure of the CO adduct **2a** in the geometry obtained by the static DFT optimization, at a temperature of 300 K. To obtain a thermal distribution of vibrational modes, the temperature was gradually increased (via rescaling of ionic velocities) by small steps. Due to the computed low-energy barriers, we did not apply any constraints to the molecular motion, allowing all the degrees of freedom to evolve naturally in time. The total time span of the simulation was 7.5 ps. To describe the reaction mechanism of the CO migratory insertion and of the following methyl-to-acyl

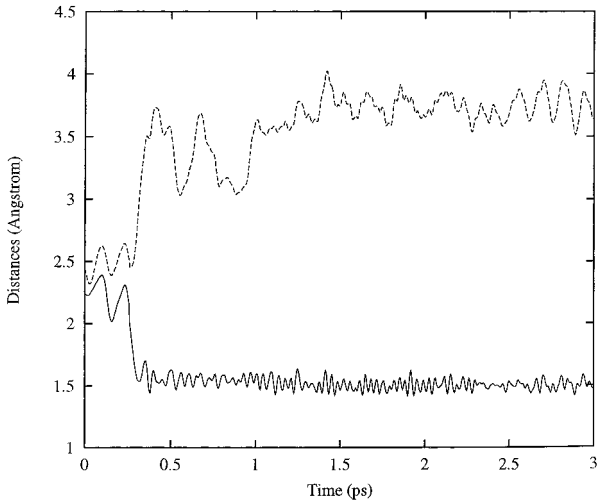

Figure 5. Time evolution of the $C_\alpha-C$ (inserting CH_3-CO), solid line, and $C_\alpha-Zr$, dashed line, distances for the time span going from 0 to 3.0 ps. Time in ps and distances in Å.

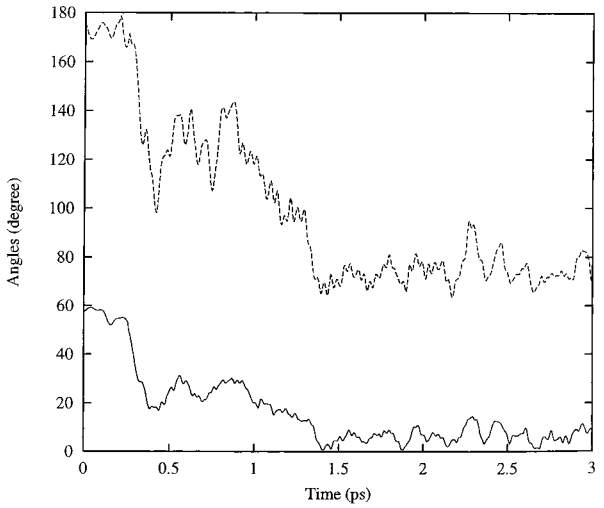

Figure 6. Time evolution of the $C_\alpha-Zr-C$ (inserting CH_3-CO), solid line, and of the $O-C-Zr$ (carbonyl), dashed line, angles for the time span going from 0 to 3.0 ps. Time in ps and angles in deg.

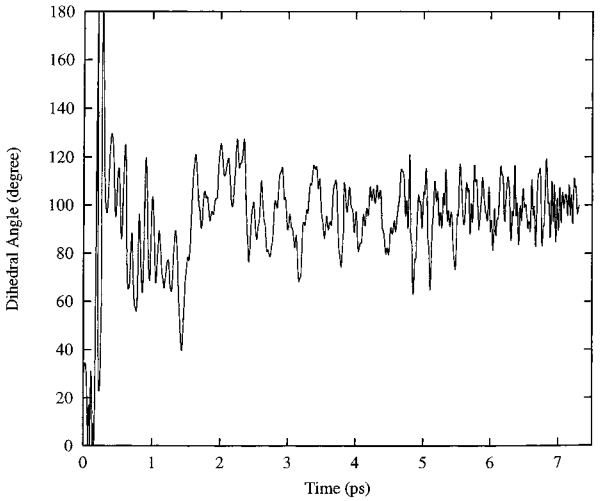

Figure 7. Time evolution of the $\angle OCZrC_\beta$ dihedral angle for the time span going from 0 to 7.5 ps. Time in ps and angle in deg.

migration in more detail, we have divided the total time span of the simulation into two portions, the first one going from 0 to 3.0 ps and the second one going from 3.0 up to 7.5 ps.

The evolution of the CO migratory insertion can be followed by studying the time evolution of several geometrical parameters, such as the $C_\alpha-C(CO)$ distance and the $Zr-C_\alpha(Me)$ distance. Indeed, the $C_\alpha-C$ distance is ca. 2.2 Å in the reagent **2a**, where the two carbon atoms belong to two different ligands, while it is only ca. 1.5 Å in the acyl product, where they are directly bound. The $Zr-C_\alpha$ distance is ca. 2.5 Å in the reagent, while it grows to ca. 3.0 and 3.7 Å in the η^1- and η^2-acyl products, respectively, where the CH_3 group and the metal are no longer bound. Figure 5 displays the variation of the $C_\alpha-C$ distance and the $Zr-C_\alpha$ distance as a function of the simulation time and clearly shows that the reactive CO migration takes place within ca. 0.5 ps. Indeed, a fast decrease in the $C_\alpha-C$ distance from ca. 2.4 to ca. 1.5 Å is observed around 0.3 ps. Thereafter, the $C_\alpha-C$ distance varies within the normal limits of a carbon−carbon vibration. At the same time the $Zr-C_\alpha$ distance follows an almost complementary trajectory with respect to the $C_\alpha-C$ distance and grows from ca. 2.5 up to ca. 3.7 Å. However, this parameter shows higher oscillations throughout the observation time, since, at the end of the reaction, the Zr and CH_3 groups are no longer bound. The achievement of the CO migration is confirmed by the time evolution of the $\angle C_\alpha-Zr-C(CO)$ angle plotted in Figure 6, which decreases from ca. 60°, close to its equilibrium value in **2a**, to ca. 20°, within 0.5 ps, reflecting the approach of the carbonyl to the methyl group. Moreover, this parameter further decreases to an average value of ca. 7°, oscillating around this value after 1.5 ps. To rationalize whether a possible facial η^1-acyl structure plays some role as a reaction intermediate, we have analyzed the evolution of the $\angle O-C-Zr$ angle as a function of the simulation time. Indeed, the chosen parameter characterizes both the CO adduct **2a** and the acyl complexes **3** and **4a**, decreasing from ca. 180° to ca. 140° to ca. 70°, on going from the CO adduct **2a** to an eventual η^1-acyl to the facial η^2-acyl complex, respectively. The $\angle O-C-Zr$ angle has been plotted as a function of the simulation time in Figure 6, from which it is clear that the CO migratory insertion leads initially to the η^1-acyl complex, which then rearranges to an η^2-structure. Indeed, a decrease in the $\angle O-C-Zr$ angle from 180° (corresponding to **2a**) to ca. 130° (characteristic of the η^1-acyl complex) is observed within 0.5 ps following the CO migration. The considered angle subsequently evolves, after 1.0 ps, toward a value of ca. 70° (characteristic of the η^2-acyl complex, **4a**) and then oscillates around this equilibrium value. The short stability of the η^1-isomer (ca. 1 ps) suggests a negligible barrier for the conversion of the η^1- into the η^2-acyl, the same result already found for the corresponding bis(cyclopentadienyl) system.[27]

To study the conformation of the incoming acyl complex, we have plotted the time evolution of the $\angle OCZrC_\beta(Me)$ dihedral angle in Figure 7, for the entire time span from 0 to 7.5 ps. This parameter characterizes the orientation of the acyl group oxygen with respect to the noninserting methyl group in the acyl complex and assumes a value of 0° and 180°, respectively, for the in-plane O-outside and O-inside conformers and a value

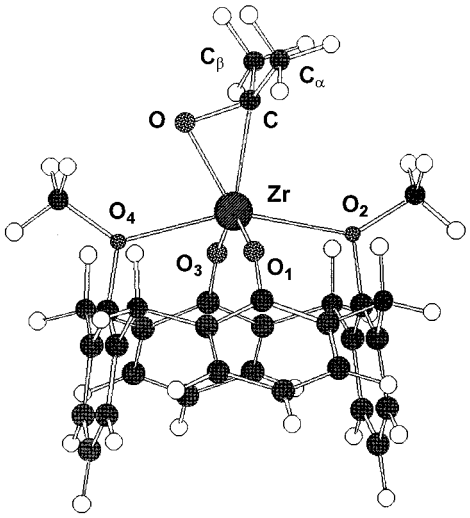

5

Figure 8. Optimized structure of the η^2-acetone complex **5**.

close to 90° for an out-of-plane conformer. From Figure 7 it appears that the migratory insertion reaction leads directly to the out-of-plane η^1- and η^2-acyl conformers; indeed, after an initial wide oscillation corresponding to the insertion reaction, the selected parameter oscillates between 60° and 120°, with an average value of 93.6° after 0.5 ps, characteristic of the out-of-plane acyl conformers (97.5° for **4a**), reaching a minimum in correspondence of the conversion from the η^1- to the η^2-acyl species, which we have identified to occur at ca. 1.5 ps (see above).

Formation of the η^2-Acetone. We optimized the geometry of the η^2-bound acetone complex **5** under C_s symmetry, finding a structure 41.1 kcal/mol lower than the facial η^2-acyl complex **4a**, therefore 71.6 kcal/mol lower than the free reagents. The CO acyl axis was directed in the plane containing the methyl groups and the metal atom, the same orientation observed in the structurally characterized [*p*-Bu^t-calix[4]-$(OMe)_2$-$(O)_2ZrCO(CH_2Ph)_2$] complex.[14] We also optimized the structure with the CO axis perpendicular to the above Me−Zr−Me plane, finding it 27.2 kcal/mol higher in energy. The minimum energy structure in Figure 8 shows that the η^2-bound acetone distorts the $\{O_4\}$ core from the planarity typical of the cone conformation of metal calix[4]arene;[31] in particular the rather short Zr−O_1 and Zr−O_3 bond distances and the large Zr−O_1−C_1 and Zr−O_3−C_3 bond angles, close to linearity, reveal a multiple Zr−O bond. A detailed list of optimized geometrical parameters, computed with both the ADF and CP programs, can be found in Table 3 together with experimental values for [*p*-Bu^t-calix[4]aren$(OMe)_2(O)_2$Zr-$(CO)(CH_2Ph)_2$], the closest compound that has been structurally characterized. We see that, as already observed for **1**, the two sets of optimized parameters are in good agreement with the experimental values; the only significant discrepancies with X-ray data are found in the $\angle O_1ZrO_3$ angle, probably because of the presence of the benzyl instead of methyl groups in the experimental complex.

Table 3. Optimized Geometrical Parameters of {[Calix[4]O_2(OMe)$_2$]Zr$(CH_3)_2$(CO)}, 5, Compared with X-ray Data of Experimental Compound {[*p*-Bu^t-calix[4]O_2(OMe)$_2$]Zr$(CH_2Ph)_2$(CO)}[14]

parameter	ADF	CP	expt[14]
R_{ZrO_1}	2.046	2.011	1.966(6)
R_{ZrO_2}	2.389	2.387	2.314(7)
R_{ZrO_4}	2.451	2.426	2.323(8)
R_{Zr-CO}	2.231	2.222	2.210(12)
R_{Zr-O}	2.026	1.995	2.084(11)
R_{C-O}	1.409	1.439	1.32(2)
$R_{C_\alpha-C}$	1.551	1.517	
$\angle O_1ZrO_3$	134.4	131.6	120.2
$\angle O_2ZrO_4$	155.4	154.4	153.1(3)
$\angle CZrO$	38.3	39.5	35.5(4)
$\angle ZrCO$	62.9	61.7	67.0(7)
$\angle C_\alpha CC_\beta$	112.9	113.4	

We then performed a linear search for the methyl-to-acyl migration starting from **4a**, by scanning the potential energy surface assuming the C_β(Me)−CO distance as a reaction coordinate in the range 3.0−1.6 Å. The potential energy curve (see Figure S3) shows a maximum of 6.6 kcal/mol with respect to reactant **4a**, for a carbon−carbon distance of ca. 2.1 Å. Starting from the maximum energy structure, we optimized the geometry of the transition state TS $_{4a\rightarrow5}$ for the methyl to acyl migration, finding a structure only 2.3 kcal/mol higher than the acyl complex **4a**. The computed structure shows an increase of 5° in the $\angle OCZrC_\beta$ dihedral angle, a decrease of 7° in the $\angle C_\alpha ZrC_\beta$ angle, and a slight increase in the C_β−Zr distance (see Table 2), with respect to **4a**. This suggets that the methyl attack occurs perpendicular to the acyl plane, with the acyl group sligthly rotated with respect to the orientation observed in **4a**, to minimize the electrostatic repulsion between the acyl oxygen and the migrating methyl. It is worth noting that the value of the energy barrier computed in the present case, 2.3 kcal/mol, is much smaller than that calculated at the same level of theory for the corresponding methyl-to-acyl migration in the Cp_2Zr-$(Me)_2(\eta^2$-$CH_3CO)$ system, 24.9 kcal/mol.[27] This energy barrier difference (22.6 kcal/mol) is remarkable and responsible for the different chemical behavior of the two systems. Indeed while Zr bis(cyclopentadienyl) η^2-acyl complexes have been isolated and structurally characterized,[10] no Zr calix[4]arene η^2-acyl could be intercepted.[14] However the existence of transient η^2-acyl intermediates in the calixarene system is supported by the experimental evidence for the analogous reaction of insertion of RCN into [*p*-Bu^t-calix[4]-$(OMe)_2(O)_2$Zr-$(R)_2$]. Indeed, in this case, bis-η^2-imminoacyl complexes have been intercepted and structurally characterized[14] and show a spatial arrangement of the η^2-imminoacyl moiety comparable to that calculated in this work for the η^2-acyl species **4a**.

To provide a rationale for such a difference, frontier orbital analysis were performed on the η^2-acyl complex **4a** and on the corresponding bis(cyclopentadienyl) complex $Cp_2Zr(Me)(\eta^2$-COMe), in the most stable O-inside geometry.[27] Both complexes show a low-lying LUMO with π^*_{CO} character, perpendicular to the acyl plane, which determines the electrophilic character of the acyl carbon.[32] At the same time the migrating C_β atom of

(31) Fantacci, S.; Sgamellotti, A.; Re, N.; Floriani, C. *Inorg. Chem.* **2001**, *40*, 1544.

(32) Tatsumi, K.; Nakamura, A.; Hofmann, P.; Stauffert, P.; Hoffmann, R. *J. Am. Chem. Soc.* **1985**, *107*, 4440.

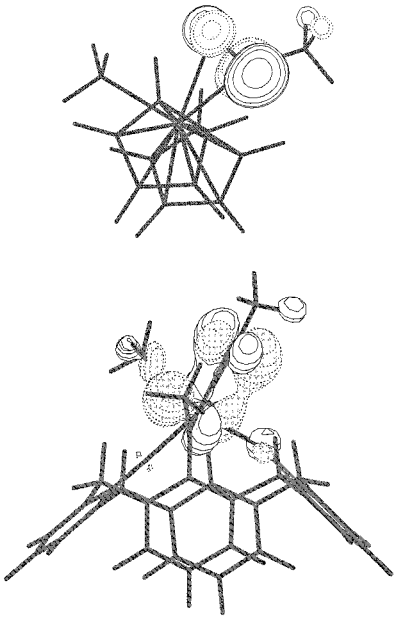

Figure 9. Isodensity surface plot of the LUMO orbitals of $Cp_2Zr(Me)(\eta^2\text{-COMe})$ and $[calix[4]\text{-}(OMe)_2(O)_2Zr(Me)(\eta^2\text{-COMe})]$.

calixarene and the bis(cyclopentadienyl) complex has a nucleophilic character, as shown by the negative Mulliken charges (−0.639 and −1.030, respectively). A comparison of the frontier orbitals of the bis(methoxycalixarene) and bis(cyclopentadienyl) η^2-acyl complexes shows that the π^*_{CO} LUMO has a lower energy in the calixarene complex (−2.43 vs −2.02 eV),[27] confirming the different behavior of the two metal fragments with respect to the methyl migration. Moreover in the calixarene η^2-acyl complex **4a** the π^*_{CO} orbital points toward the methyl (C_β) substituent, while in the bis(cyclopentadienyl) complex the π^*_{CO} is perpendicular to the plane containing the methyl group; see Figure 9. Therefore, both the energy and the spatial orientation of the LUMO of the calixarene η^2-acyl complex **4a** favor the attack of the migrating methyl, leading easily to the η^2-ketone complex.

The energy profile for the overall reaction leading to the acetone complex **5** has been reported in Figure 10 and shows that all steps are exothermic and present negligible energy barriers.

Dynamics Calculations. The dynamics of the methyl migration can be followed by studying the time evolution of the C_β−CO (acyl and methyl) distance and of the Zr−C_β distance. Indeed, the C_β−CO distance is ca. 3.0 Å in the reagent **4a**, where the two carbon atoms belong to two different ligands, while it is only ca. 1.5 Å in the acyl product, where they are directly bound; on the other hand, the Zr−C_β distance is ca. 2.4 Å in complex **4a**, where the methyl is bound to the metal, while it grows to ca. 3.3 Å in the η^2-acetone complex **5**, where the methyl is detached from the metal. In Figure 11 the two selected parameters have been plotted as a function of the simulation time, for the time span going from 3.0 to 7.5 ps. As it can be noticed, the methyl migration takes place within 5.0 ps, as outlined by the fast decrease in the CO−C_β distance, observed around 4.7 ps, which after 5.0 ps oscillates within the limits of a normal carbon−carbon vibration. Moreover, the Zr−C_β distance shows a fast increase in correspondence of 4.7 ps from ca. 2.4 Å, close to its equilibrium value in **4a**, to ca. 3.3 Å, characteristic of the product **5**, reflecting the detachment of the methyl group from the metal center upon methyl migration. It is interesting to observe how the carbonyl C−O distance, plotted in Figure 11 as a function of the simulation time, varies accordingly in correspondence with the migration reaction, increasing from a value of ca. 1.25 Å, characteristic of the η^2-acyl complex **4a**, up to ca. 1.45 Å upon formation of the η^2-acetone, reflecting the stronger Zr → CO π back-donation in the latter Zr(II) d^2 complex with respect to the Zr(IV) d^0 methyl acyl complex **4a**. The achievement of the methyl-to-acyl migration is

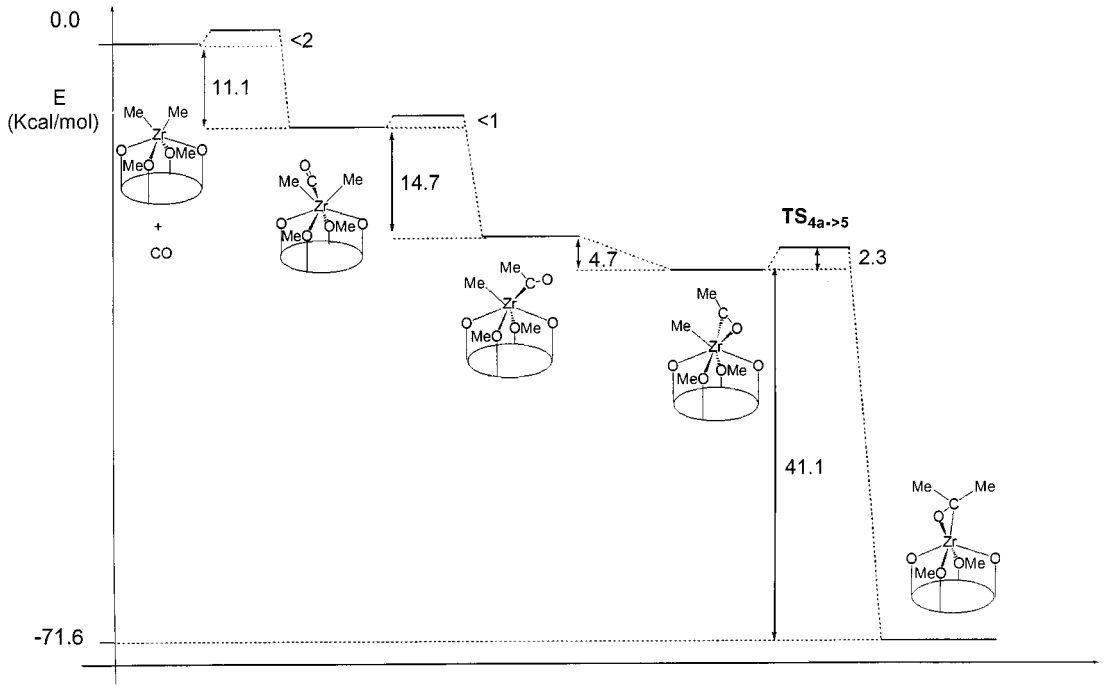

Figure 10. Energetics of the whole multistep CO migratory insertion.

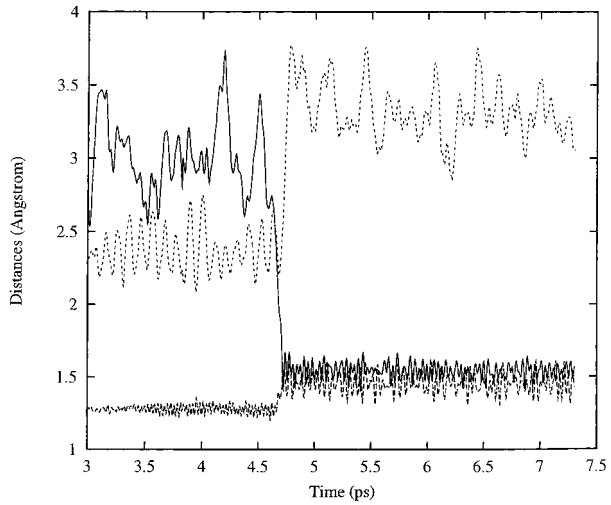

Figure 11. Time evolution of the $C_\beta-CO$ (solid), $Zr-C_\beta$ (dashed), and C−O (dots) distances, for the time span going from 3.0 to 7.5 ps. Time in ps and distances in Å.

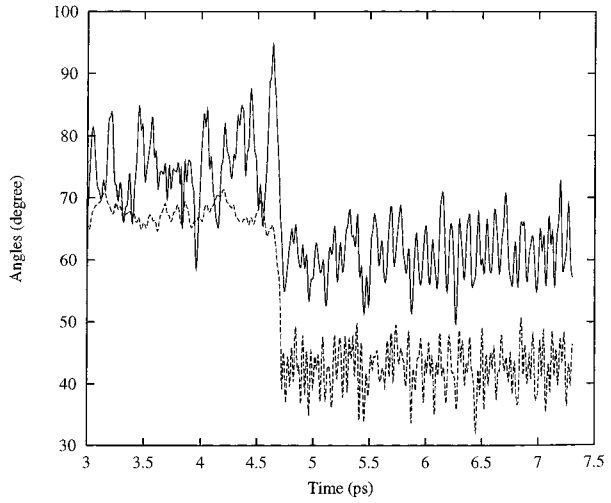

Figure 12. Time evolution of the $\angle C_\beta ZrC(CO)$ (dashed) and ∠OCZr (solid) angles, for the time span going from 3.0 to 7.5 ps. Time in ps and angles in deg.

confirmed by the time evolution of the $\angle C_\beta ZrC(CO)$ (inserting methyl−acyl) angle, plotted in Figure 12, which shows a fast decrease around 4.5 ps from a value of ca. 70°, close to its equilibrium value in the complex **4a**, to ca. 40°, characteristic of the η^2-bound acetone **5**, reflecting the approach of the methyl to the acyl group and the formation of the new carbon−carbon bond. To check whether a possible η^1-acyl isomer plays some role in the methyl migration process, we have analyzed the evolution of the ∠OCZr (acyl carbon) angle as a function of the simulation time. The results, plotted in Figure 12, show that the migrating methyl attacks directly the η^2-coordinated acyl group; indeed, no opening in the ∠OCZr angle is observed before the methyl migration happens, even if a fluctuation of this parameter up to ca. 95° accompanies the methyl attack. Moreover, from Figure 7 it can be noticed that the migrating methyl attacks directly the out-of-plane η^2-acyl isomer **4a**; indeed, no significant variations in the $\angle C_\beta ZrCO$ dihedral angle are observed in correspondence with the methyl migration, confirming that the methyl attack occurs perpendicular to the acyl plane, as suggested by the frontier orbital picture exposed above.

Conclusions

The multistep migratory insertion of CO into the Zr−CH_3 bond of [calix[4](OMe)$_2$(O)$_2$ZrMe$_2$] has been investigated combining static DFT calculations on the stationary points of the potential surface (see Figure 10 for a summary of the results) with first-principles molecular dynamics calculations based on the Car−Parrinello method. Frontier orbital analysis performed on the [calix[4](OMe)$_2$(O)$_2$ZrMe$_2$] complex **1**, shows an isolated LUMO directed along the line bisecting the Me−Zr−Me plane, which, at variance with the $(Cp)_2Zr(Me)_2$ system, results in the formation of the facial [calix[4](OMe)$_2$(O)$_2$ZrMe$_2$−CO] complex **2a** as the only stable CO adduct.

Molecular dynamics simulations, performed starting from complex **2a**, have shown that the migratory insertion of CO into the zirconium−methyl bond leads as a preliminary product to a facial η^1-acyl complex **3**, which further relaxes to the corresponding η^2-bound isomer **4a** within 1.5 ps, in agreement with the computed relative stability of the η^1- and η^2-bound acyl isomers; see Figure 10.

The final reaction product, the η^2-bound acetone complex **5**, was found 71.6 kcal/mol below the energy of the free reagents, with a barrier for the methyl migration of only 2.3 kcal/mol; such a small value, 22.6 kcal/mol lower than that for the $(Cp)_2Zr(Me)(\eta^2$-COMe) system, is due to the different energy and spatial orientation of the LUMO of reactant **4a**, which points toward the migrating methyl favoring the facial CH_3 attack (see Figure 9). Moreover, molecular dynamics simulations performed starting from **4a** confirm that the methyl migration takes place by a direct attack of the CH_3 group to the facial η^2-acyl complex **4a**, without the intermediacy of any η^1-acyl isomers.

We conclude that the investigated migratory insertion reaction leads to a η^2-bound acetone via a labile η^2-acyl complex, providing a rationale for the experimental evidence that no η^2-acyl complexes were detected as isolable intermediates in the reaction of [*p*-Bu^t-calix[4](OMe)$_2$(O)$_2$ZrMe$_2$] with CO, at variance with the corresponding $(Cp)_2Zr(Me)_2$ system.

Acknowledgment. We wish to thank Dr. Paolo Giannozzi for generating the Zr pseudopotential. We thank Dr. Francesco Mercuri for helpful discussions. F.D.A. wishes to thank the CNR (Programma "Short-term mobility", year 2000) for financial support. Thanks are due to the CNR (Progetto Finalizzato "Materiali Speciali per Tecnologie Avanzate II").

Supporting Information Available: Potential energy profiles for CO coordination, CO insertion, and methyl-to-acyl migration (PS). This material is available free of charge via the Internet at http://www.pubs.acs.org.

OM010509I